PRECLINICAL AND CLINICAL IMAGING – Full Papers

Magnetic Resonance in Medicine 78:1488–1495 (2017)

Hepatic Function Imaging Using Dynamic Gd-EOB-DTPA Enhanced MRI and Pharmacokinetic Modeling

Jia Ning,[1†] Zhiying Yang,[2†] Sheng Xie,[3] Yongliang Sun,[2] Chun Yuan,[1,4] and Huijun Chen[1]*

Purpose: To determine whether pharmacokinetic modeling parameters with different output assumptions of dynamic contrast–enhanced MRI (DCE-MRI) using Gd-EOB-DTPA correlate with serum-based liver function tests, and compare the goodness of fit of the different output assumptions.

Methods: A 6-min DCE-MRI protocol was performed in 38 patients. Four dual-input two-compartment models with different output assumptions and a published one-compartment model were used to calculate hepatic function parameters. The Akaike information criterion fitting error was used to evaluate the goodness of fit. Imaging-based hepatic function parameters were compared with blood chemistry using correlation with multiple comparison correction.

Results: The dual-input two-compartment model assuming venous flow equals arterial flow plus portal venous flow and no bile duct output better described the liver tissue enhancement with low fitting error and high correlation with blood chemistry. The relative uptake rate K_i^r derived from this model was found to be significantly correlated with direct bilirubin ($r = -0.52$, $P = 0.015$), prealbumin concentration ($r = 0.58$, $P = 0.015$), and prothrombin time ($r = -0.51$, $P = 0.026$).

Conclusion: It is feasible to evaluate hepatic function by proper output assumptions. The relative uptake rate has the potential to serve as a biomarker of function. **Magn Reson Med 78:1488–1495, 2017. © 2016 International Society for Magnetic Resonance in Medicine.**

Key words: different output assumptions; pharmacokinetic modeling; Gd-EOB-DTPA; function evaluation

INTRODUCTION

Hepatic function evaluation is important in preoperative planning for liver surgery (1). Serum bilirubin (total bilirubin (TBil) and direct bilirubin (DBil)) and certain proteins (albumin (Alb), prealbumin (PA) concentration, and prothrombin time (PT)) are used widely in clinical practice to quantify the liver function, because they reflect the function of liver (2,3). However, quantification of regional liver function is more important in surgery planning (4). Thus, medical imaging methods with localized function evaluation have been proposed. For example, technetium-99m diethylenetriaminepenta acid galactosyl human serum albumin (^{99m}Tc-GSA) clearance, which reflects the liver function, quantified by single photon emission computed tomography (SPECT) has been found to be correlated with indocyanine green (ICG) retention rate–related liver function (5). However, it suffers from low clinical availability, ionizing radiation exposure, and low spatial resolution.

Recently, dynamic contrast enhanced (DCE) MR imaging with a hepatobiliary contrast agent, Gd-EOB-DTPA, has been proposed to quantify hepatic functions (6,7). Gd-EOB-DTPA can not only permeate into the extravascular extracellular space (EES), but also be transported into hepatocytes through polypeptides organic anion transporter OATP1B1 and OATP1B3, and then be excreted by multidrug resistance protein MRP2 through bile (8,9). The pharmacokinetics of Gd-EOB-DTPA provides a good opportunity to quantify regional hepatic function, because the transfer and excretion rate directly reflect the hepatic function. First, descriptive parameters were proposed using a simple imaging protocol with limited dynamic phases (10). However, the descriptive parameters do not have physical meanings and cannot model the real hepatic pharmacokinetics of Gd-EOB-DTPA. Recently, a dual-input two-compartment model was proposed and investigated (11). However, the hepatic function parameters generated from pharmacokinetic modeling of DCE-MRI with Gd-EOB-DTPA have not been validated with clinical serum-based liver function tests. Moreover, the most suitable assumptions of this model are still needed to be determined with a clinical available imaging protocol, including the output assumptions of contrast excretion through bile and veins.

The purpose of this study is to use the 6-min dynamic Gd-EOB-DTPA–enhanced MRI protocol to fit four dual-input two-compartment models with different output assumptions and a one-compartment model known as the Van Beers model (12) to determine whether hepatic function parameters quantified by pharmacokinetic modeling correlate with serum-based liver function tests, and to compare goodness of fit using the Akaike information criterion (AIC) fitting error.

THEORY

Based on the previously developed dual-input two-compartment model (11), we further discussed the outputs of models based on the pharmacokinetics of the contrast and

[1]Center for Biomedical Imaging Research, Department of Biomedical Engineering, School of Medicine, Tsinghua University, Beijing, China.

[2]Department of Hepatobiliary Surgery, China-Japan Friendship Hospital, Beijing, China.

[3]Department of Radiology, China-Japan Friendship Hospital, Beijing, China.

[4]Department of Radiology, University of Washington, Seattle, Washington, USA.

Grant sponsor: National Natural Science Foundation of China; Grant numbers: 81571667; 81371540.

*Correspondence to: Huijun Chen, PhD, Center for Biomedical Imaging Research, Department of Biomedical Engineering, School of Medicine, Tsinghua University, Beijing 100084, China. Tel: + 86 10-62798332; E-mail: chenhj_cbir@mail.tsinghua.edu.cn.

†These authors contributed equally to this work.

Received 19 June 2016; revised 17 September 2016; accepted 28 September 2016

DOI 10.1002/mrm.26520

Published online 26 October 2016 in Wiley Online Library (wileyonlinelibrary.com).

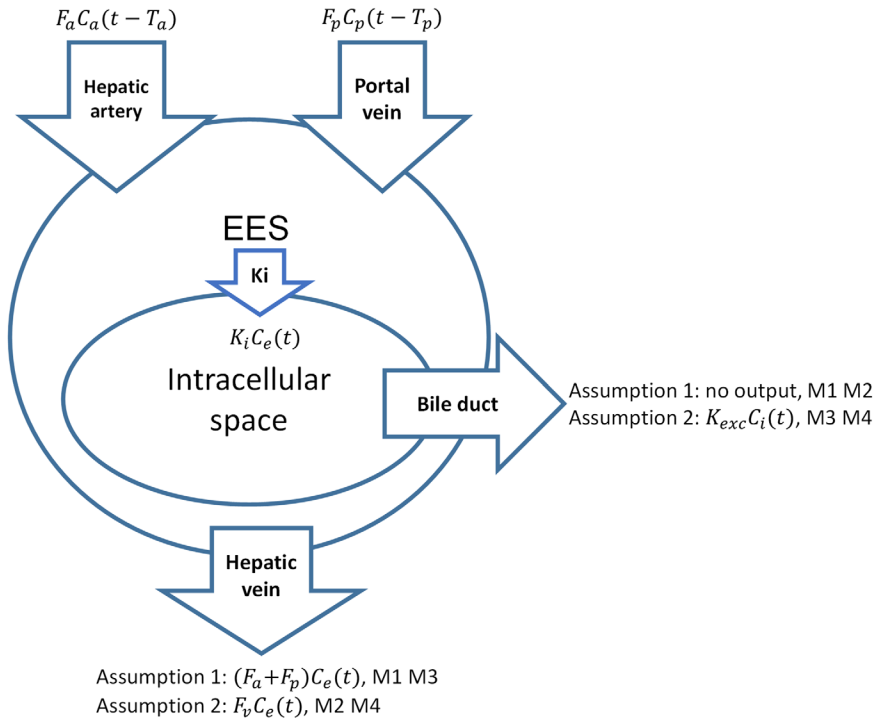

FIG. 1. Diagram of the pharmacokinetic models with different assumptions investigated in this study. Contrast was taken into the EES by arterial flow F_a with concentration C_a and portal venous flow F_p with concentration C_p, considering time delays, T_a and T_p, respectively. Then, the contrast enters the intracellular space from the EES with a constant intracellular uptake rate K_i. At the same time, part of contrast flows out through the venous flow F_v (assumption 1) or $F_a + F_p$ (assumption 2) with contrast concentration C_e. For the compartment of intracellular space with concentration C_i, we assume no bile excretion (assumption 1) or part of excretion via bile with a fixed excretion rate K_{exc} (assumption 2).

imaging protocol. The models investigated in this study are composed of two compartments: the EES and intracellular space. The whole pharmacokinetic process of Gd-EOB-DTPA (13–15) is show in Figure 1. For an EES compartment with concentration $C_e(t)$, there are two inputs: the inflow from the hepatic artery F_a with concentration $C_a(t - T_a)$, and the portal venous inflow F_p with concentration $C_p(t - T_p)$), in which T_a and T_p are the arterial and portal venous delay, respectively. Usually, T_p can be neglected (11), as the region of interest (ROI) of portal venous input function (PIF) we selected was much nearer than that of arterial input function (AIF). Considering the contrast outputs from EES, one output connects the intracellular space with a fixed intracellular uptake rate K_i; another output flows out through the hepatic vein F_v with concentration $C_v(t)$. $C_e(t)$ is used as a substitute of $C_v(t)$ (11), because it is difficult to directly measure $C_v(t)$ from images because of the complicated structure of the hepatic vein. Here, the hepatic venous flow F_v can be directly fitted, or can be assumed to be $F_a + F_p$ (11). For an intracellular compartment with concentration $C_i(t)$, the contrast input is from EES with the uptake rate K_i, and output through the bile duct, which can be assumed to have a fixed excretion rate K_{exc} (9,16), or the bile output can be ignored because of the short total acquisition duration (11).

Finally, the total contrast concentration of hepatic parenchyma can be represented by $C_t(t) = V_iC_i(t) + V_eC_e(t)$, where V_e and V_i are the volume fractions of EES and the intracellular space, respectively. Thus, four pharmacokinetic models (M1–M4) can be derived from two possible assumptions of venous output, $(F_a + F_p)C_e(t)$ (M1, M3) or $F_vC_e(t)$ (M2, M4); and two assumptions of bile duct output: no output (M1, M2), or $K_{exc}C_i(t)$ (M3, M4). The derived model equations are as follows:

M1 (11):

$$C_t(t) = \left(K_i/V_e + \delta(t)\right) \otimes \left(F_aC_a(t - T_a) + F_pC_p(t - T_p)\right) \otimes \exp\left(-(F_a + F_p + K_i)t/V_e\right) \quad [1]$$

M2:

$$C_t(t) = \left(K_i/V_e + \delta(t)\right) \otimes \left(F_aC_a(t - T_a) + F_pC_p(t - T_p)\right) \otimes \exp\left(-(F_v + K_i)t/V_e\right) \quad [2]$$

M3:

$$C_t(t) = \left(K_i\exp(-K_{exc}t/V_i)/V_e + \delta(t)\right) \otimes \left(F_aC_a(t - T_a) + F_pC_p(t - T_p)\right) \otimes \exp\left(-(F_a + F_p + K_i)t/V_e\right) \quad [3]$$

M4:

$$C_t(t) = \left(K_i\exp(-K_{exc}t/V_i)/V_e + \delta(t)\right) \otimes \left(F_aC_a(t - T_a) + F_pC_p(t - T_p)\right) \otimes \exp\left(-(F_v + K_i)t/V_e\right) \quad [4]$$

For liver function evaluation, the previously published uptake rate K_i and uptake fraction $f_i = K_i/(F_a + F_p + K_i)$ are reported. Two additional hepatic function parameter

are proposed and tested in this study: the relative uptake rate $K_i^r = K_i/V_e$ and the relative excretion rate $K_{exc}^r = K_{exc}/V_i$. For perfusion evaluation, the arterial inflow F_a, portal venous inflow F_p, and the arterial flow fraction $AF = F_a/(F_a + F_p)$ are derived. The generated parameters include

M1: $K_i, f_i, K_i^r, F_a, F_p$, and AF
M2: K_i^r, F_a, F_p, and AF
M3: $K_i, f_i, K_i^r, K_{exc}^r, F_a, F_p$, and AF
M4: $K_i^r, K_{exc}^r, F_a, F_p$, and AF.

METHODS

Data Acquisition

To evaluate the fitting performance of models with different assumptions, 38 patients (19 men, 19 women; mean age 51.3 ± 11.3 years; range 31–74 years) who were suspected to have liver lesions, referred to having MR imaging, and willing to participate, were recruited between December 2012 and December 2013. This study was approved by the institutional review board, and written informed consent was obtained from all patients. All of the patients had no contraindications to receive MRI scans with Gd-EOB-DTPA injection, no sign of masses compressing the main trunk of the vessels, no cavernous transformation of the portal vein, and no biliary obstruction.

All patients were imaged on a 3.0 Tesla (T) scanner (Discovery MR750, GE Healthcare, Milwaukee, Wisconsin, USA) with an 8-channel phase-array torso coil (HDMR2 RX, GE Healthcare). DCE-MR images were acquired with a clinically available T_1-weighted 3D gradient-echo sequence (Liver Accelerated Volume Acquisition (LAVA), GE Healthcare) with the following scan parameters: 40 axial slices with 5-mm thickness, 3-mm in-plane resolution, 2.08-ms repetition time, 0.82-ms echo time, 12° flip angle, 400-mm field of view, 256 reconstruction matrix size, 128 acquisition matrix size, 90% phase field of view, 0.71 number of averages, 976.56-Hz pixel bandwidth, 2-s temporal resolution, 6-min total duration time. Coincident with the first scan, 0.025-mmol/kg Gd-EOB-DTPA (gadoxetic acid, Primovist; Bayer, Leverkusen, Germany) was injected intravenously by a power injector at 2 mL/s and followed by a 15 mL saline flush at the same rate. During the whole scan, patients were instructed to breathe quietly.

The blood chemistry tests and hepatitis tests, including hepatitis B virus and hepatitis C virus, were performed within 3 days of the MRI exam for all of the patients. The liver function–related tests included TBil, DBil, Alb, PA, and PT.

Data Analysis

Blind to the patient information and blood chemistry results, the ROIs were drawn manually for each subject to acquire AIF, PIF, and three hepatic lobe enhancement curves with a custom-designed software in MATLAB (R2011b, The MathWorks, Natick, Massachusetts, USA). Rectangle ROIs were generated around seed pixels chosen by the reviewer. All ROIs were also adjusted phase by phase to avoid partial volume artifacts, motion artifacts, and to compensate the misregistration among phases. To extract vascular functions including AIF $C_a(t)$ and PIF $C_p(t)$, a cluster-based method was used. First, the seed point for each ROI was carefully selected to capture the maximal enhancement and void artifacts on the image of the most enhanced phase. Then all of the pixels in each ROI were classified into five clusters using the fuzzy c-means cluster algorithm. The mean profile of the cluster most correlated (Pearson correlation) with the seed point was used. For $C_a(t)$ extraction, an ROI was drawn in the aorta at the level of porta hepatis. The $C_p(t)$ was obtained from an ROI inside the intrahepatic part of the portal vein. Finally, three ROIs were selected as evenly distributed as possible on the left, middle, and right hepatic lobes for each case, avoiding the blood vessel, tumor, edema, and lesion. To improve the signal to noise ratio, the mean intensity was used for the hepatic parenchyma ROIs.

Examples of selected ROIs for AIF, PIF, and hepatic parenchyma of a patient (female, 41 years old) are shown in Figures 2a–2c, respectively. With the assumption of a linear relationship between the image intensity and the contrast concentration (11,17–19), a relative enhancement curve $RE(t) = (S(t) - S(0))/S(0)$ was used in model fitting, in which $S(t)$ is the image intensity of the t th phase, and $t = 0$ represents the precontrast phase. The nonlinear least-squares curve fitting routine lsqcurvefit (20) in MATLAB was used for model fitting with fixed initial value. AIC fitting error was used to evaluate the goodness of fit for each model (21). To simplify the fitting, the portal venous delay T_p was set to zero, and the best fit was identified for the arterial delay T_a ranging from 0–20 s in increments of 1 s (11). The numbers of parameters directly derived from model fitting of M1, M2, M3, and M4 were 4 (F_a, F_p, K_i, V_e), 4 (F_a, F_p, F_v/V_e, K_i^r), 5 (F_a, F_p, K_i, V_e, K_{exc}^r), and 5 (F_a, F_p, F_v/V_e, K_i^r, K_{exc}^r), respectively.

As a comparison, the previous published dual-input single compartment model, the Van Beers model (12), was also fitted to obtain F_a, F_p, and AF. The Van Beers model ignores the intracellular compartment, and assumes an outflow rate K_o, which is

$$C_t(t) = \Big(F_a C_a(t - T_a) + F_p C_p(t - T_p)\Big) \otimes \exp(-K_o t) \quad [5]$$

All of the continuous variables were presented as means ± standard deviation (SD) or median with interquartile range (IQR) according to whether the data conformed to a normal distribution (22). The Spearman or Pearson correlation was used to compare the pharmacokinetic parameters and blood chemistry parameters as appropriate. Holm's procedure was used for multiple comparison correction (23). Moreover, the student's t-test was employed to compare the means of AIC fitting error among models.

RESULTS

All patients were successfully imaged and analyzed. The final diagnosis of these patients included hepatocellular carcinoma (HCC), hemangioma, cholangiocarcinoma, hepatic metastasis, hepatic lymphoma, and other hepatic benign masses. The median (IQR) or mean ± SD of Alb, PA, TBil,

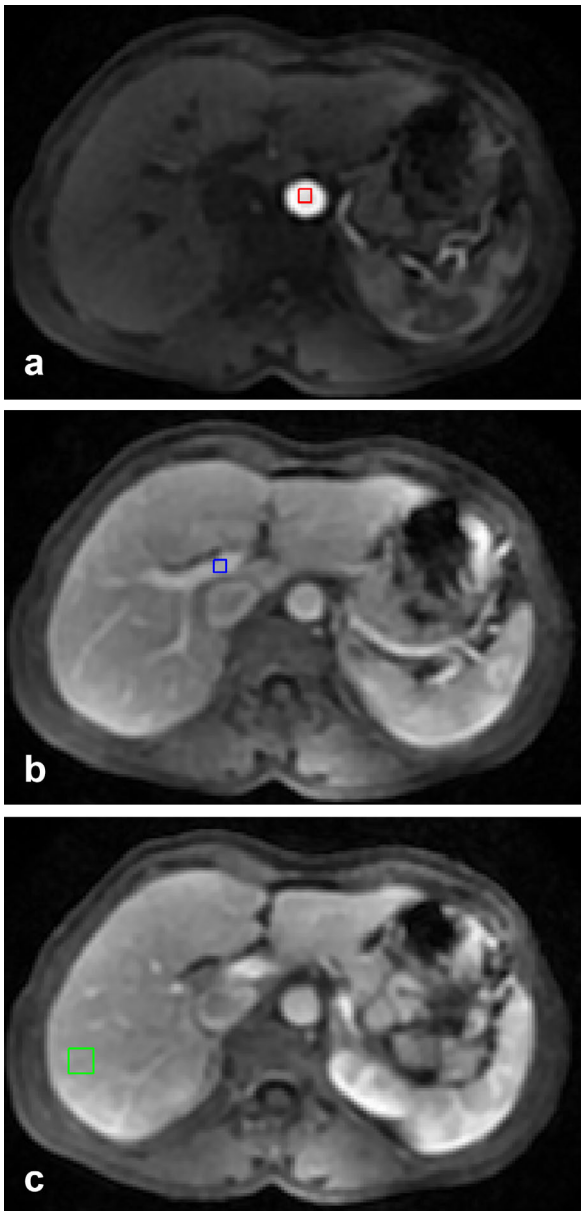

FIG. 2. Sample ROI selection in dynamic Gd-EOB-DTPA–enhanced images of a 41-year-old female with inflammatory lesions: (a) AIF (red rectangle); (b) PIF (blue rectangle); (c) hepatic parenchyma (green rectangle).

DBil, and PT was 42.68 ± 4.74 g/L (n = 38), 0.20 ± 0.08 mg/L (n = 38), 10.7 (8.3) μmol/L (n = 38), 3.75 (2.8) μmol/L (n = 38), and 13.15 (1.1) s (n = 34), respectively. Figure 3a shows examples of AIF and PIF derived from the same patient as shown in Figure 2. The corresponding hepatic parenchyma enhancement fitting results of all of the models are given in Figure 3b. The fitted curves of the Van Beers model and M3 showed obvious mismatch with the acquired data. Significant differences were found for AIC fitting errors between different models, as shown in Figure 4. The Van Beers model had the largest fitting error compared with M1–M4 ($P < 0.001$ for all of the models). Among M1–M4, the AIC fitting errors of M1 and M4 had no significant difference ($P = 0.872$) and were significantly lower than M2 and M3 ($P < 0.001$).

The hepatic function parameters (K_i, K_i^r, f_i, and K_{exc}^r) calculated from M1–M4 in this heterogeneous population is summarized in Table 1. The uptake rate K_i and uptake fraction f_i generated from M1 has similar values with published results (11). M3 calculated lower K_i and f_i than M1 with the assumption of bile output. For the proposed relative uptake rate K_i^r, values fitted by all models were on the same order of magnitude. With the relative excretion rate K_{exc}^r, M3 calculated unrealistic high values, whereas M4 has much smaller values.

Table 2 gives the perfusion parameters for all models. Van Beers calculated the largest arterial flow F_a and portal venous flow F_p. High blood inflow was also found in M2. The blood inflow parameters (F_a and F_p) of M1 and M4 are similar in order of magnitude, and the AF values are higher than M2. M3 generated unreasonable dominating arterial perfusion F_a with minimum portal venous flow F_p.

The correlation between the pharmacokinetic hepatic function parameters and blood chemistry parameters are given in Table 3. Function parameters derived from M1, M2, and M4 showed weak to moderate (abs (r): 0.33–0.58) significant correlations with some blood chemistry

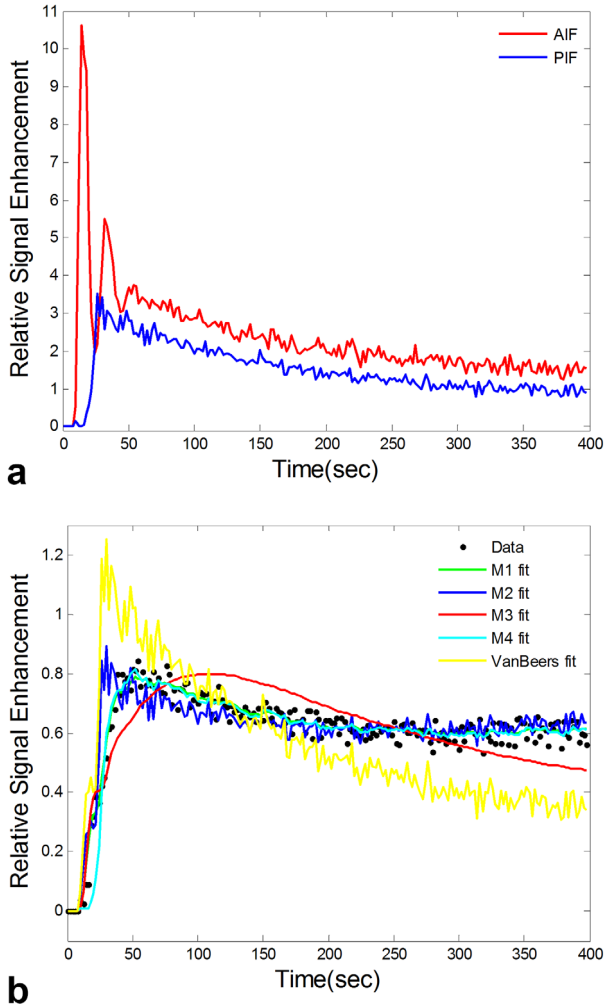

FIG. 3. Examples of (**a**) AIF, PIF, and (**b**) acquired hepatic parenchyma data extracted from the ROIs shown in Figure 2 for the same patient, and the fitted curves for all investigated models.

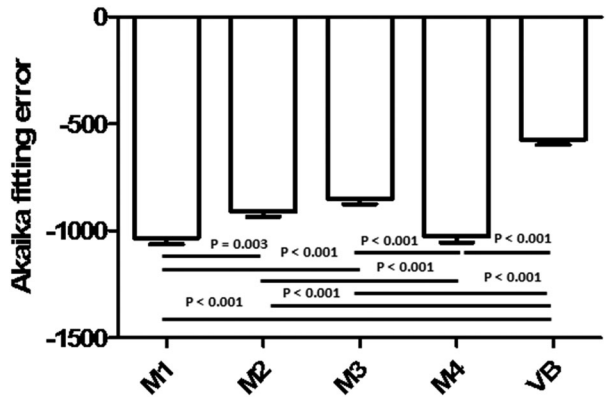

FIG. 4. AIC fitting errors of different models (column, mean value; bar on each column, standard deviation). The line connecting every two models indicates that there is a significant difference ($P < 0.05$ in student's t-test) between them.

parameters. Among all model parameters, the proposed relative uptake rate K_i^r derived from M1 was significantly correlated with blood chemistry parameters, including DBil ($r = -0.52$, $P < 0.001$), Alb ($r = 0.43$, $P = 0.007$), PA ($r = 0.58$, $P < 0.001$), and PT ($r = -0.51$, $P = 0.002$). After multiple comparison correction, it was still significantly correlated with DBil ($P = 0.015$), PA ($P = 0.015$), and PT ($P = 0.026$). K_i^r of M2 also exhibited similar significant correlations with DBil ($r = -0.47$, $P = 0.003$), Alb ($r = 0.42$, $P = 0.009$), PA ($r = 0.54$, $P < 0.001$), and PT ($r = -0.51$, $P = 0.002$). After multiple comparison correction, the significant correlations remained with DBil ($P = 0.009$), Alb ($P = 0.018$), PA ($P = 0.005$), and PT ($P = 0.008$). Other than that, the hepatic uptake fraction f_i fitted by M1 was found to be weakly correlated with DBil, PA and PT; the intracellular uptake rate K_i calculated from M1 is weakly correlated with DBil and PT; and K_i^r and K_{exc}^r from M4 were weakly correlated with DBil and PA, respectively. However, the significance of these correlations was gone after a multiple comparison correction. No significant correlation was found between the function parameters calculated from M3 and the blood chemistry.

Table 4 summarizes the significant correlations found between the perfusion parameters of all models and the blood chemistry tests without multiple comparison correction.

Table 1
Distribution of Hepatic Function Parameter Fitting for M1–M4

Model	Hepatic function parameter	Data[a]
M1	K_i (/100/min)	4.72 (2.97)
	K_i^r (/min)	0.40 ± 0.15
	f_i (%)	10.02 ± 5.03
M2	K_i^r (/min)	0.56 ± 0.19
M3	K_i (/100/min)	0.92 (2.34)
	K_i^r (/min)	0.73 (0.26)
	K_{exc}^r (/min)	465 ± 150
	f_i (%)	2.63 (7.06)
M4	K_i^r (/min)	0.64 (0.28)
	K_{exc}^r (/min)	0.08 (0.12)

[a]Data were the median with interquartile range (IQR) or means ± SD as appropriate.

Table 2
Distribution of Perfusion Parameter Fitting for All Models

Model	Parameter	Data[a]
M1	F_a (mL/100mL/min)	18.0 (12.0)
	F_p (mL/100mL/min)	30.0 (26.7)
	AF (%)	45.36 ± 22.19
M2	F_a (mL/100 mL /min)	61.0 (37.3)
	F_p (mL/100 mL /min)	246.2 ± 55.5
	AF (%)	20.99 ± 9.80
M3	F_a (mL/100 mL /min)	13.5 (5.6)
	F_p (mL/100 mL /min)	0.1 (11.3)
	AF (%)	99.49 (27.10)
M4	F_a (mL/100 mL /min)	15.1 (14.0)
	F_p (mL/100 mL /min)	39.7 (40.4)
	AF (%)	35.95 ± 20.20
Van Beers	F_a (mL/100 mL /min)	183.0 (173.9)
	F_p (mL/100 mL /min)	404.0 (329.0)
	AF (%)	32.01 ± 21.39

[a]Data were median with interquartile range (IQR) or means ± SD as appropriate.

The arterial flow F_a derived from M1 was weakly correlated with TBil. Weak correlations were also found between portal venous flow F_p of M2 and PA, the AF of M4 and TBil, AF of Van Beers, and PT. Although perfusion parameters generated from M3 had unrealistic values, F_a was found to be weakly correlated with PA and Alb, and F_p correlated with Alb. However, no significant correlation was found between the perfusion parameters and the blood chemistry tests after multiple comparison correction.

DISCUSSION

In this study, the hepatic function parameters derived from liver dynamic Gd-EOB-DTPA–enhanced MRI using dual-input two-compartment models were found to significantly correlate with blood chemistry tests with reasonable physiological interpretations (24). Among all blood chemistry tests, DBil, PT, and PA are sensitive and specific indicators for liver function in clinical practice. An increase of DBil results from impaired liver function, because DBil is metabolized by liver (2,3). However, both PA and PT reflect the protein synthesis function of liver. Decreased PA is closely related to early decrease in nutritional status caused by liver function damage (2,3,25), whereas prolonged PT indicates the lack of clotting factors that are synthesized by liver (26). Thus, the negative correlations of pharmacokinetic function parameters found with DBil and PT, and the positive correlations found with PA, further confirm the feasibility of pharmacokinetic modeling of DCE-MRI with hepatobiliary contrast in liver function evaluation. Notably, this study validated the methodology in a heterogeneous population with heterogeneous hepatic function, emphasizing its value and usability in patients with different physiologically conditions.

Among all of the pharmacokinetic parameters, the proposed relative uptake rate K_i^r was found to have the highest correlations with blood chemistry tests in M1 and M2, indicating that it could be a good parameter for hepatic function evaluation. Although previous studies proposed intracellular uptake rate K_i and derived hepatic uptake fraction f_i (11) as functional parameters to reflect

Table 3
Correlation between the Imaging Hepatic Function Parameters and Blood Chemistry

Model/ Parameter		DBil		TBil		Alb		PA		PT	
		Correlation coefficient	*P* value	Correlation coefficient	*P* value	Correlation coefficient	*P* value	Correlation coefficient	*P* value	Correlation coefficient	*P* value
M1	K_i	−0.43[a]	0.007	−0.28	0.085	0.17	0.310	0.27	0.096	−0.39[a]	0.024
	f_i	−0.33[a]	0.044	−0.21	0.202	0.21	0.206	0.34[a]	0.035	−0.46[a]	0.006
	K_i^r	−0.52[b]	<0.001	−0.23	0.163	0.43[a]	0.007	0.58[b]	<0.001	−0.51[b]	0.002
M2	K_i^r	−0.47[b]	0.003	−0.20	0.238	0.42[b]	0.009	0.54[b]	<0.001	−0.51[b]	0.002
M3	K_i	−0.04	0.785	−0.03	0.821	−0.18	0.265	−0.15	0.377	0.25	0.156
	f_i	−0.15	0.378	−0.04	0.819	0.03	0.842	0.01	0.935	0.17	0.336
	K_{exc}^r	−0.16	0.335	0.08	0.647	0.14	0.404	0.15	0.373	−0.11	0.547
	K_i^r	0.02	0.905	0.06	0.703	−0.17	0.293	−0.16	0.328	0.29	0.099
M4	K_i^r	−0.36[a]	0.026	−0.07	0.665	0.23	0.163	0.21	0.209	−0.24	0.179
	K_{exc}^r	0.20	0.221	0.12	0.461	−0.26	0.120	−0.40[a]	0.014	0.19	0.294

[a]Significant ($P \leq 0.05$ without multiple comparison correction).
[b]Significant after multiple comparison correction.

hepatic functions, our results suggested that K_i^r could be a better parameter for liver function quantification by eliminating the influence of EES volume fraction V_e. The reason may be that effective EES volume (V_e), where a contrast agent can permeate into, will change in a damaged liver because the liver cell density will decrease and the extracellular matrix will increase through several mechanisms (27,28) in the liver damage process.

In this study, four dual-input two-compartment models with different output assumptions (M1–M4) and a dual-input one-compartment model (Van Beers model) were compared. The results showed that adding the intracellular compartment is necessary to fit the real DCE-MRI data using Gd-EOB-DTPA, which echoes a previous investigation (11). However, taking the bile duct output into consideration may introduce large fitting errors (M3) or poor reflection of hepatic function (M3 and M4). The reason may be that the relative slow transport rate of Gd-EOB-DTPA makes the bile duct excretion effect difficult to observe within the 6-min data acquisition used in this study, supported by the fact that the enhancement in bile duct can only be observed 10 min after contrast injection (29,30). The unrealistic fitting results of the relative excretion rate K_{exc}^r in M3 and the bad performance of K_{exc}^r of M4 in blood chemistry validation further suggest that assuming a fixed bile duct output may not be suitable for a short-time DCE protocol. With respect to the vein output assumption, fitting F_v alone (M2) increased the fitting error and deceased the function parameters produced (K_i and f_i were unavailable) compared with assuming $F_v = F_a + F_p$ (M1), but both methods have similar performance to produce clinical relevant hepatic function parameter K_i^r. However, the reason for the high fitting error in M2 may also be caused by using $F_v C_e$ as an approximation of $F_v C_v$. Because C_v is not readily available from the DCE images, the alternative C_e could introduce a large deviation from the reality. Future efforts should more appropriately account for hepatic venous outflow and concentration. However, as a one-compartment model, the Van Beers model has much higher perfusion parameters compared with other models. The biggest reason is that it cannot describe the pharmacokinetics of Gd-EOB-DTPA with the single-compartment assumption, resulting in nonphysical fitting results. Considering all aspects, the dual-input two-compartment model with no bile duct output and $F_v = F_a + F_p$ assumption (M1) has the best performance in goodness of fit and correlations with blood chemistry in this study.

Table 4
Significant Correlations ($P \leq 0.05$, without Multiple Comparison Correction) Found between the Perfusion Parameters and the Blood Chemistry

Model	Parameter pair	Correlation coefficient[a]	*P* value
M1	F_a versus TBil	0.37	0.021
M2	F_p versus PA	−0.37	0.023
M3	F_a versus PA	−0.41	0.009
	F_p versus Alb	−0.35	0.031
	F_a versus Alb	−0.33	0.042
M4	AF versus TBil	0.35	0.030
Van Beers	AF versus PT	0.39	0.023

[a]Correlations were Spearman rank or Pearson correlation as appropriate.

In the analysis of dynamic Gd-EOB-DTPA–enhanced MRI, the pharmacokinetic model can not only quantify hepatic function evaluation, but also calculate the perfusion parameters of liver, including the arterial flow F_a, the venous flow F_p, and arterial flow fraction AF. Previous studies has found that the increase of arterial flow F_a or arterial flow fraction AF were associated with hepatic function damage (18,31,32). In this study, although we found some weak correlations between those perfusion parameters and blood chemistry tests, thus supporting the previous finding, those relationships were not significant after multiple comparison correction.

There are limitations to this study. First, the liver function parameters quantified by pharmacokinetic modeling of DCE-MRI were measured using the uptake of Gd-EOB-DTPA, which was directly related to the OATP transporters expression (8,33). However, the blood chemistry tests, which reflect the biosynthesis function of liver, were used as a reference in this study because of the unavailability of transporters expression data. However, previous studies have proven that subjects with impaired liver function, such as advanced fibrosis or hepatitis, have decreased OATP

expression (34,35). The technical limitation of this study is that DCE images were acquired on free-breathing subjects with a clinical available sequence, suffering from misregistration among dynamic phases, even severe motion and artifacts in some images. Consequently, a careful ROI selection criterion was used instead of pixel-wise analysis to avoid introducing bias caused by motion and artifacts. Although we chose three ROIs distributed as evenly as possible on liver tissue for each case, the whole liver function cannot be fully quantified to some degree, which may affect the results. Thus, a motion-insensitive imaging sequence, such as the radial sampling technique (36,37) and nonrigid registration for postprocessing, are needed in future studies to generate pixel-wise function parameter maps, which is more valuable for preoperative planning. Another technical limitation is that we used the relative enhancement curves by assuming a linear relationship between intensity and contrast concentration (11,17–19), rather than estimating contrast concentration directly from the T_1 change, which may introduce bias in the pharmacokinetic analysis.

In conclusion, through validation with blood chemistry, pharmacokinetic analysis of dynamic Gd-EOB-DTPA–enhanced MRI offers the possibility to quantitatively access regional liver function reserve for surgery planning. The dual-input two-compartment model with the assumptions of no bile duct output and venous flow equals arterial flow plus portal venous flow can better model the Gd-EOB-DTPA enhancement in hepatic parenchyma.

ACKNOWLEDGMENTS

The authors thank Daniel S. Hippe (Department of Radiology, University of Washington) for his help in statistical consulting. They also thank Timothy J. Colgan (Department of Radiology, University of Wisconsin-Madison), for language check and polishing.

REFERENCES

1. Guglielmi A, Ruzzenente A, Conci S, Valdegamberi A, Iacono C. How much remnant is enough in liver resection? Digest Surg 2012; 29:6–17.
2. Green RM, Flamm S. AGA technical review on the evaluation of liver chemistry tests. Gastroenterology 2002;123:1367–1384.
3. Thapa BR, Walia A. Liver function tests and their interpretation. Indian J Pediatr 2007;74:663–671.
4. Yoshida M, Beppu T, Shiraishi S, Tsuda N, Sakamoto F, Okabe H, Hayashi H, Baba H, Yamashita Y. 99mTc-GSA SPECT/CT fused images for assessment of hepatic function and hepatectomy planning. Ann Trans Med 2015;3.
5. Hwang E-H, Taki J, Shuke N, Nakajima K, Kinuya S, Konishi S, Michigishi T, Aburano T, Tonami N. Preoperative assessment of residual hepatic functional reserve using 99mTc-DTPA-galactosyl-human serum albumin dynamic SPECT. J Nucl Med 1999;40:1644–1651.
6. Ryeom H-K, Kim S-H, Kim J-Y, Kim H-J, Lee J-M, Chang Y-M, Kim Y-S, Kang D-S. Quantitative evaluation of liver function with MRI using Gd-EOB-DTPA. Korean J Radiol 2004;5:231–239.
7. Katsube T, Okada M, Kumano S, Hori M, Imaoka I, Ishii K, Kudo M, Kitagaki H, Murakami T. Estimation of liver function using T1 mapping on Gd-EOB-DTPA-enhanced magnetic resonance imaging. Invest Radiol 2011;46:277–283.
8. Van Beers BE, Pastor CM, Hussain HK. Primovist, Eovist: what to expect? J Hepatol 2012;57:421–429.
9. Hamm B, Staks T, Mühler A, Bollow M, Taupitz M, Frenzel T, Wolf K-J, Weinmann H-J, Lange L. Phase I clinical evaluation of Gd-EOB-DTPA as a hepatobiliary MR contrast agent: safety, pharmacokinetics, and MR imaging. Radiology 1995;195:785–792.
10. Wibmer A, Prusa AM, Nolz R, Gruenberger T, Schindl M, Ba-Ssalamah A. Liver failure after major liver resection: risk assessment by using preoperative gadoxetic acid–enhanced 3-T MR imaging. Radiology 2013;269:777–786.
11. Sourbron S, Sommer WH, Reiser MF, Zech CJ. Combined quantification of liver perfusion and function with dynamic gadoxetic acid–enhanced MR imaging. Radiology 2012;263:874–883.
12. Materne R, Smith AM, Peeters F, Dehoux JP, Keyeux A, Horsmans Y, Van Beers BE. Assessment of hepatic perfusion parameters with dynamic MRI. Magn Reson Med 2002;47:135–142.
13. König J, Nies AT, Cui Y, Leier I, Keppler D. Conjugate export pumps of the multidrug resistance protein (MRP) family: localization, substrate specificity, and MRP2-mediated drug resistance. Biochimica et Biophysica Acta (BBA)-Biomembranes 1999;1461:377–394.
14. Muhler A, Elferink RPO, Weinmann H-J. Complete elimination of the hepatobiliary MR contrast agent Gd-EOB-DTPA in hepatic dysfunction: an experimental study using transport-deficient, mutant rats. Magma 1993;1:134–139.
15. Narita M, Hatano E, Arizono S, Miyagawa-Hayashino A, Isoda H, Kitamura K, Taura K, Yasuchika K, Nitta T, Ikai I. Expression of OATP1B3 determines uptake of Gd-EOB-DTPA in hepatocellular carcinoma. J Gastroenterol 2009;44:793–798.
16. Spinazzi A, Lorusso V, Pirovano G, Kirchin M. Safety, tolerance, biodistribution, and MR imaging enhancement of the liver with gadobenate dimeglumine: results of clinical pharmacologic and pilot imaging studies in nonpatient and patient volunteers. Acad Radiol 1999;6:282–291.
17. Saito K, Ledsam J, Sourbron S, Otaka J, Araki Y, Akata S, Tokuuye K. Assessing liver function using dynamic Gd-EOB-DTPA-enhanced MRI with a standard 5-phase imaging protocol. J Magn Reson imaging 2013;37:1109–1114.
18. Hagiwara M, Rusinek H, Lee VS, Losada M, Bannan MA, Krinsky GA, Taouli B. Advanced liver fibrosis: diagnosis with 3D whole-liver perfusion MR imaging—initial experience 1. Radiology 2008;246: 926–934.
19. Do RKG, Rusinek H, Taouli B. Dynamic contrast-enhanced MR imaging of the liver: current status and future directions. Magn Reson Imaging Clin N Am 2009;17:339–349.
20. Gaens ME, Backes WH, Rozel S, Lipperts M, Sanders SN, Jaspers K, Cleutjens JP, Sluimer JC, Heeneman S, Daemen MJ. Dynamic contrast-enhanced MR imaging of carotid atherosclerotic plaque: model selection, reproducibility, and validation. Radiology 2013;266: 271–279.
21. Banerji A, Naish JH, Watson Y, Jayson GC, Buonaccorsi GA, Parker GJ. DCE-MRI model selection for investigating disruption of microvascular function in livers with metastatic disease. J Magn Reson Imaging 2012;35:196–203.
22. Lang TA, Secic M. How to Report Statistics in Medicine: Annotated Guidelines for Authors, Editors, and Reviewers. Minneapolis, MN: ACP Press, 2006.
23. Holm S. A simple sequentially rejective multiple test procedure. Scand J Stat 1979;6:65–70.
24. Balzan S, Belghiti J, Farges O, Ogata S, Sauvanet A, Delefosse D, Durand F. The "50-50 criteria" on postoperative day 5: an accurate predictor of liver failure and death after hepatectomy. Ann Surg 2005;242:824.
25. Saito M, Seo Y, Yano Y, Miki A, Yoshida M, Azuma T. Short-term reductions in non-protein respiratory quotient and prealbumin can be associated with the long-term deterioration of liver function after transcatheter arterial chemoembolization in patients with hepatocellular carcinoma. J Gastroenterol 2012;47:704–714.
26. Knight JA. Liver function tests: their role in the diagnosis of hepatobiliary diseases. J Infusion Nurs 2005;28:108–117.
27. Yang C, Zeisberg M, Mosterman B, Sudhakar A, Yerramalla U, Holthaus K, Xu L, Eng F, Afdhal N, Kalluri R. Liver fibrosis: insights into migration of hepatic stellate cells in response to extracellular matrix and growth factors. Gastroenterology 2003;124:147–159.
28. Moreira RK. Hepatic stellate cells and liver fibrosis. Arch Pathol Lab Med 2007;131:1728.
29. Saito S, Obata A, Kashiwagi Y, Abe K, Murase K. Dynamic contrast-enhanced MRI of the liver in Mrp2-Deficient rats using the hepatobiliary contrast agent Gd-EOB-DTPA. Invest Radiol 2013;48:548–553.
30. Norén B, Dahlström N, Forsgren MF, Leinhard OD, Kechagias S, Almer S, Wirell S, Smedby Ö, Lundberg P. Visual assessment of biliary excretion of Gd-EOB-DTPA in patients with suspected diffuse

liver disease—a biopsy-verified prospective study. Eur J Radiol Open 2015;2:19–25.
31. Chen BB, Hsu CY, Yu CW, Wei SY, Kao JH, Lee HS, Shih TT. Dynamic contrast-enhanced magnetic resonance imaging with Gd-EOB-DTPA for the evaluation of liver fibrosis in chronic hepatitis patients. Eur Radiol 2012;22:171–180.
32. Baxter S, Wang ZJ, Joe BN, Qayyum A, Taouli B, Yeh BM. Timing bolus dynamic contrast-enhanced (DCE) MRI assessment of hepatic perfusion: initial experience. J Magn Reson Imaging 2009;29: 1317–1322.
33. Leonhardt M, Keiser M, Oswald S, Kühn J, Jia J, Grube M, Kroemer HK, Siegmund W, Weitschies W. Hepatic uptake of the magnetic resonance imaging contrast agent Gd-EOB-DTPA: role of human organic anion transporters. Drug Metab Dispos 2010;38:1024–1028.
34. Nakai K, Tanaka H, Hanada K, Ogata H, Suzuki F, Kumada H, Miyajima A, Ishida S, Sunouchi M, Habano W. Decreased expression of cytochromes P450 1A2, 2E1, and 3A4 and drug transporters Na+-taurocholate-cotransporting polypeptide, organic cation transporter 1, and organic anion-transporting peptide-C correlates with the progression of liver fibrosis in chronic hepatitis C patients. Drug Metab Dispos 2008;36:1786–1793.
35. Svoboda M, Riha J, Wlcek K, Jaeger W, Thalhammer T. Organic anion transporting polypeptides (OATPs): regulation of expression and function. Curr Drug Metab 2011;12:139–153.
36. Feng L, Grimm R, Block KT, Chandarana H, Kim S, Xu J, Axel L, Sodickson DK, Otazo R. Golden-angle radial sparse parallel MRI: combination of compressed sensing, parallel imaging, and golden-angle radial sampling for fast and flexible dynamic volumetric MRI. Magn Reson Med 2014;72:707–717.
37. Kim KW, Lee JM, Jeon YS, Kang SE, Baek JH, Han JK, Choi BI, Bang Y-J, Kiefer B, Block KT. Free-breathing dynamic contrast-enhanced MRI of the abdomen and chest using a radial gradient echo sequence with K-space weighted image contrast (KWIC). Eur Radiol 2013;23: 1352–1360.